SSC22-WKP2-13

Design of 6U Nanosatellites in Formation Flying for the Laser Crosslink Mission

Geuk-Nam Kim*, Sang-Young Park, Han-Gyeol Ryu, Young-Eon Kim,
Suyong Choi, Joohee Lee, Sungmoon Lee, Seuggwon Jeon
Department of Astronomy, Yonsei University, Seoul, Republic of Korea
614A, 50 Yonsei-ro, Seodaemun-gu, Seoul, Republic of Korea; +82 2 2123 4442
south1003@yonsei.ac.kr

Sehyun Seong
Telepix Co., Ltd., Busan, Republic of Korea
302, 435-1 Haeyang-ro, Yeongdo-gu, Busan, Republic of Korea; +82 51 731 2884
shseong@telepix.net

ABSTRACT

With a recent growth in the volume of spaceborne data, free space optical (FSO) or laser communication systems are attracting attention, as they can enable super-high data rates faster than 1 Gbps. The Very high-speed Inter-satellite link Systems using Infrared Optical terminal and Nanosatellite (VISION) is a technical demonstration mission to establish and validate laser crosslink systems using two 6U nanosatellites in formation flying. The final goal is to achieve a Gbps-level data rate at a distance of thousands of kilometers. To establish space-to-space laser communication, the payload optical axes of each satellite should be precisely aligned during the crosslink. The payload is the laser communication terminal (LCT) including the deployable space telescope (DST), which improves optical link performances. The 6U nanosatellite bus is designed with commercial off-the shelf-(COTS) components for agile systems development. For precise formation flying, the bus is equipped a with relative navigation system with a GNSS receiver and RF crosslink, star tracker, 3-axis reaction wheels (RWs), and propulsion system. This proposed concept of the laser crosslink systems will contribute to the construction of the LEO communication constellation with high speed and secure links in future.

Keywords: Laser Crosslink, Nanosatellite, Formation Flying.

INTRODUCTION

Laser communication is a promising method to deal with the recent growth in data volume transmitted by spaceborne platforms, with the potential to achieve Gbps-level data rates. The laser communication systems enhance the size, weight, and power (SWaP) efficiency compared to traditional RF systems at low cost. With a wide spectral range and narrow beam, this system improves link security and reduces the potential risk from mutual interference, jamming, and undesired signal interception from third parties. In addition, there are no regulatory constraints on licensing frequency bands, a situation that is helpful for the establishment of an LEO mega-constellation. These advantages have commercial and military applications such as high-speed data relaying in remote sensing or surveillance systems.[1] Thus, we proposed novel laser crosslink systems for the Very high-speed Inter-satellite link Systems using Infrared Optical terminal and Nanosatellite (VISION) mission. The mission aims to establish a laser crosslink system using two 6U nanosatellites in formation flying, named Altair and Vega. The final goal is to achieve a data rate of 1 Gbps at an inter-satellite distance of up to 1000 km.[2]

The payload of the laser communication terminal (LCT) consists of a seed laser, amplifier, electronics, and optics including the deployable space telescope (DST) as front-end mirrors. The DST acting as an antenna is a Cassegrain-type telescope with segmented mirrors, which can significantly enhance beam transmission and receiving gain with low power consumption. The LCT handles a single infrared laser beam for sharing data transmissions with the pointing, acquisition, and tacking (PAT) sequence. The 6U nanosatellite bus is designed with COTS, given the limited resources involved, to improve SWaP efficiency. In addition to the fine beam pointing system of the LCT, which utilizes a fast steering mirror (FSM), the nanosatellite bus provides precise pointing. To improve and maintain the crosslink, a feedback control system combines the FSM with detectors to compensate beam pointing drift due to orbital motions. The core technology for the mission is a precise formation flying guidance, navigation, and control (FFGNC) system,

including an S-band RF crosslink system and propulsion system. The nanosatellites perform precise attitude control utilizing a 3-axis reaction wheel assembly (RWA) integrated with a star tracker (STT), ensuring that tracking errors remain within tens of arcsec during the laser crosslink. The relative navigation algorithm, which uses GPS, L1, and L2, signals can improve the pointing capability by eliminating the effects of ionospheric delay. In addition, both nanosatellites are equipped with a cold gas propulsion system to adjust the inter-satellite range rapidly and accurately given mission scenarios, from 50 to 1000 km. The deployable solar panels meet the electrical power requirement, and a hinge with a self-locking mechanism can mitigate attitude control performance degradation due to jitter and flexible mode. The flight software has a modular architecture based on the core flight system (cFS), and the data interface mainly uses the CAN-bus.

In this paper, we present the preliminary design of the laser crosslink systems using 6U nanosatellites in formation flying.

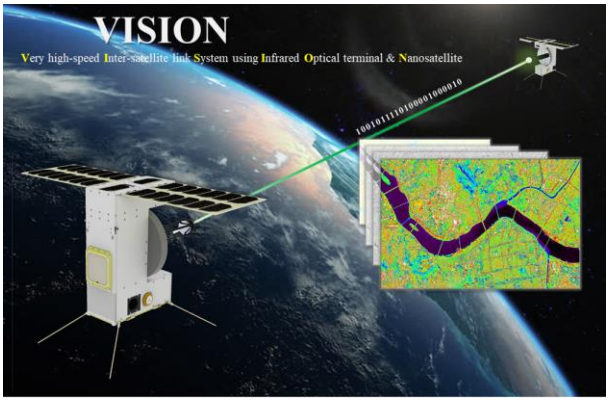

Figure 1: Illustration of the VISION mission

LASER CROSSLINK MISSION

Mission Overview

The VISION mission is aimed to demonstrate the novel laser crosslink systems with two nanosatellites, achieving a data rate of 1 Gbps at a distance of 1000 km apart. To establish the crosslink, the optical axes of each nanosatellite are precisely aligned, reducing the residual jitters about the line-of-sight (LOS) to be smaller than 1 μrad, thus guaranteeing good optical link performance. The mission lifetime is desired to be longer than 1 year, and the systems are contained in the 6U standard.

Concept of Operations

The mission lifetime is composed of three phases: the launch and early orbit phase (LEOP), drift recovery and station-keeping phase (DRSKP), and normal operation phase (NOP). The phases comprise several modes for systems check-out, commissioning, telecommunication, and maneuvers.

The concept of operations (ConOps) of the nanosatellites is presented in Figure 2. After being ejected in orbit, they drift several thousand kilometers away, operating independently. Through orbit maneuvers in the DRSKP, the inter-satellite distance is changed by several kilometers. During the NOP, they sequentially adjust inter-satellite ranges from 50 to 1000 km and conduct laser crosslink tests.

In the LEOP, the nanosatellites are set to the standby mode by the ground telecommand after the end of detumbling. Basic operation modes like standby, communication, and safe are autonomously exchanged and activated by monitoring the system status, including parameters such as the battery capacity, temperature, and telecommand schedule. During the standby mode, the satellites are ready to receive telecommands for mode changes and time synchronization with ground station. The telemetry and mission data are downloaded during the communication mode. The safe mode handles contingencies, having the highest priority. During the commissioning, maneuver, and mission modes, operations are performed through ground telecommands. In particular, in the NOP, the commissioning mode is related to formation flying system tests, including the RF crosslink and relative navigation. Finally, the mission mode is defined as the entire sequence for the laser crosslink, detailed in the following subsection. After mode operations are completed, the satellites automatically return to the standby mode. Figure 3 depicts the operation mode flows for both satellites.

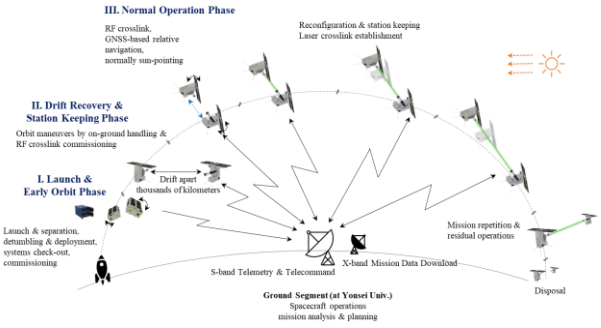

Figure 2: Concept of Operations

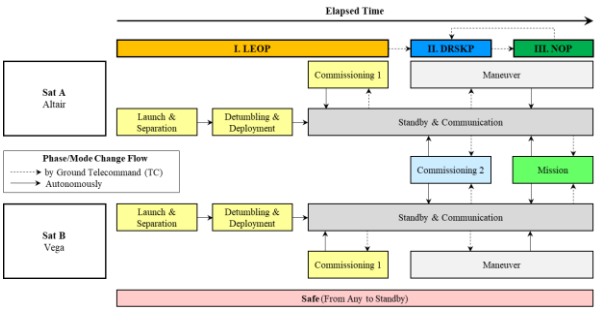

Figure 3: Diagram of mode operation flows

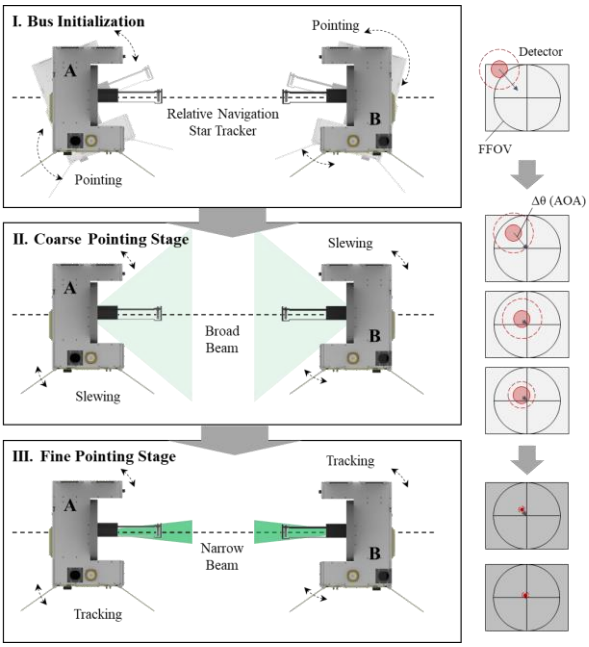

Figure 4: Concept of the PAT sequence

Pointing, Acquisition, and Tracking Sequence

To implement the laser crosslink, the LOS vectors between each payload optical axis should be aligned precisely in sub-arcseconds using attitude and FSM control, termed the PAT sequence. The PAT sequence is classified in three stages: (1) bus initialization, (2) the coarse pointing stage (CPS), and (3) the fine pointing stage (FPS). Specially, for the CPS and FPS, two types of beam divergence angles and sensors used as a beam detector are applied. One detector is the short-wave-infrared camera (SWIR CAM) detector, termed the CAM, and the other is the quadrant cell (QC) detector. Figure 4 illustrates the PAT sequence in nanosatellite orientations with various beam divergence angles and beam spot projected on the detectors.

Table 1: Descriptions of the PAT sequence

(a) Coarse Pointing Stage (CPS)

Contents	**Descriptions**		
Sub-stage	Search	Acquisition	Detection
Duration	~ 4 min		~ 1 min
Pointing Error (μ, σ) [μrad]	< (1200, 400)		
Beam Divergence	Broad / Unsteady		Broad / Steady
Actuator	RWs		RWs (FSM)
Measurement	CAM (Relative Navigation, STT, Gyro)		
Optical Link Budget Case	PAT#1	PAT#2	PAT#3

(b) Fine Pointing Stage (FPS)

Contents	**Descriptions**	
Sub-stage	Hand-off	Tracking & Communication
Duration	~ 10 min	
Pointing Error (μ, σ) [μrad]	< (30, 1)	
Beam Divergence	Narrow / Steady	
Actuator	FSM (RWs)	
Measurement	QC (CAM, Relative Navigation, STT, Gyro)	
Optical Link Budget	PAT#4	COM#1

In the bus initialization operation, the relative navigation with an S-band RF crosslink system is based on the differential GNSS algorithm and estimates the relative position and velocity with sub-meter accuracy. Using the relative position vectors, the desired LOS vectors are roughly calculated for the satellites to find each other. When the LOS error is smaller than the full field of view (FFOV) of the CAM or the field of uncertainty (FOU), they start to transmit a broad beam, entering the CPS. As shown in the middle of Figure 4, the beam spot projected on the CAM is biased owing to

errors induced by attitude determination and control, and mechanical misalignment, in which the bias is defined as the AOA (Angle of Arrival, $\Delta\theta$). The AOA can be corrected by attitude control using the CAM feedback. Then, the beam spots on both satellites stay within a threshold of the QC's FFOV. However, the platform may still jitter. To eliminate jitter residuals, the FSM is activated. In the FPS, the beam divergence angle is narrow and the QC is used for FSM feedback with high frequency measurements. Within a tip-tilt angle of the FSM, the LOS errors from the attitude maneuver and jitter residuals can be rejected, enhancing the optical link performance. For the entire PAT sequence, the bus should provide precise attitude control to align the LOS of the satellites with each other by compensating for the drift by orbital motion, which is called slewing.

The details of the PAT sequence are summarized in Table 1 according to the sub-stages. The CPS should be ended within 5 minutes, and the FPS should be maintained for over 10 minutes. In the CPS, the PAT algorithm estimates the AOA using CAM measurements to correct the bias using attitude control. After the Acquisition is finished, the FSM is available. Given the beam divergence angle, the pointing error should be smaller than 1200 μrad and 400 μrad for the bias (μ) and standard deviation errors (σ), respectively. In the FPS, the precision of the LOS jitter should be reduced to less than 1 μrad by operating the FSM. Furthermore, the relative navigation system and CAM are always enabled to prevent the satellites from missing each other.

CONCEPT OF LASER CROSSLINK SYSTEMS

Systems Architecture

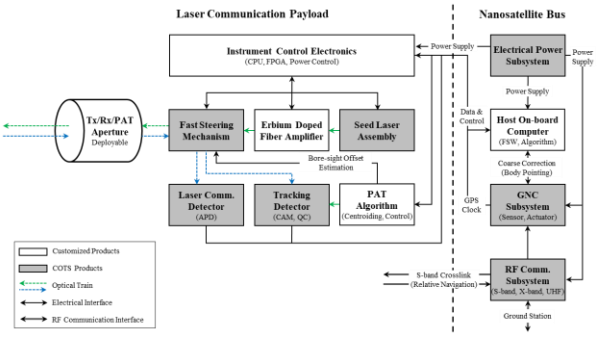

Figure 5: Diagram of the systems architecture

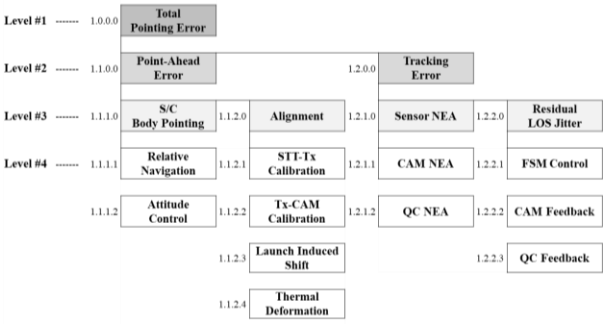

Figure 6: Pointing error budget structure

The VISION systems consist of the LCT and nanosatellite bus. Given the restricted configuration with 6U standards, the attitude maneuver of the bus acts as a gimbal system that assists the beam pointing and tracking. To overcome the constraints on the size, several parts are integrated in a single feature for miniaturization. For example, the instrument control electronics (ICE) on the LCT provide multiple functions for the PAT algorithm computation, handling instruments, and power management.

With the systems architecture adopting COTS, the systems development lifecycle is significantly reduced. In addition, the systems performance has been rapidly and quantitively estimated in the design process based on the specifications of the COTS parts. Figure 5 presents the systems architecture of the integrated laser communication payload and nanosatellite bus. The diagram describes the electrical interfaces including power supply and data communications.

Pointing Error

To achieve the Gbps level of inter-satellite data transmission at thousands of kilometers, it is necessary to secure a signal-to-noise (SNR) margin of higher than 10 dB. Pointing loss is the main cause of performance degradations of the optical link.[3]

The pointing error budget is divided into point-ahead and tracking terms, as presented in Figure 6, which shows the structure of the pointing error budget. The point-ahead errors include satellite body-pointing and misalignment of instruments, which can be corrected over the CPS. The tracking errors are related to detectors' signal noise and residual jitters, which can be reduced by the FSM over the FPS.

Payload – Laser Communication Terminal

The payload (LCT) has a monostatic architecture that shares beam paths for either communication or PAT through a single aperture. This approach enhances the

performance of FSM feedback controls and mitigates steady-state beam pointing errors.

Figure 7 displays the payload configurations and beam paths in the optical bench. The primary mirror is segmented into three parts, and the secondary mirror is attached on the boom-deployment-type baffle, saving space for the launch phase. The COTS-based optical components are arranged on the optical bench. The support plate is a mechanical interface with the bus, and is designed with Invar-36, which has high structural stiffness, to mitigate on-orbit thermal deformations.

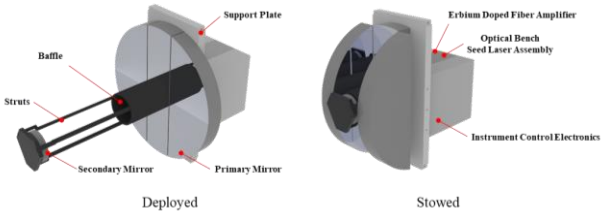

(a) Stowed and deployed exterior configuration

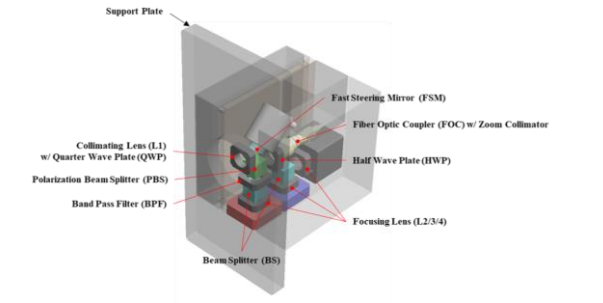

(b) Optical bench interior configuration

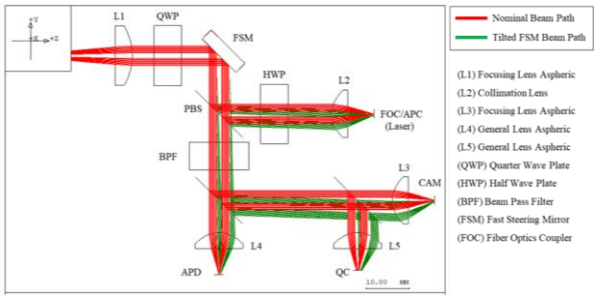

(c) Beam paths in FSM operations

Figure 7: LCT payload configurations and beam paths in optical bench

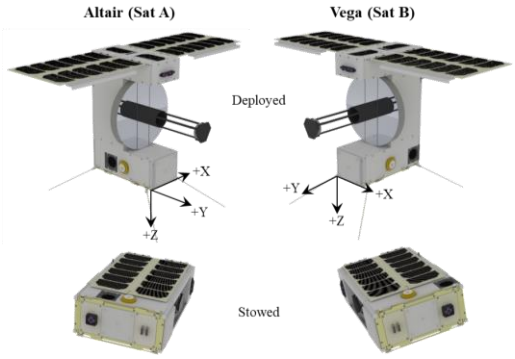

(a) Coordinate and exterior configurations

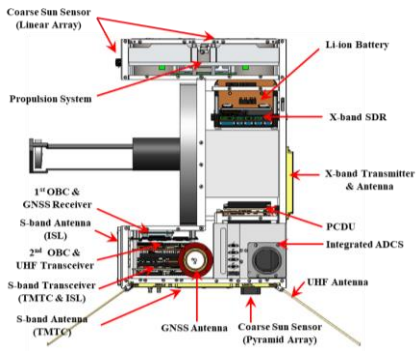

(b) interior configuration (Vega, Sat B)

Figure 8: Nanosatellite bus configurations

The nanosatellite configurations are depicted in Figure 8. Each satellite's star tracker aperture and GNSS antenna are located opposite each other to ensure good visibility of the mission operations. The integrated attitude determination and control subsystem (ADCS) is a single box containing actuators and sensors, and has its own processor for algorithm execution. Three sun sensors attached on the body Y/Z-axes are used to acquire the sun vector from any state. The two deployable solar panels can generate the electrical power required to keep the battery state of charge (SOC) over 50% even in the end of lifetime (EOL). Furthermore, the panels prevent direct sunlight incidence on the payload optics during the mission operations.

The electrical interfaces are shown in Figure 9. The panels are connected with regulators on the power conditioning and distribution unit (PCDU) for battery charging. The PDCU manages the power supply for each component, providing latch-up protection to avoid damage from overcurrent or overvoltage. By applying two-wire bus interfaces such as CAN and I^2C, the

wiring is significantly reduced compared to that of serial interfaces. To mitigate susceptibility to bus faults of the I^2C interfaces, they are only applied to internal or backup communication interfaces, including redundancy systems.

Guidance, Navigation, and Control Subsystem

The GNC subsystem is composed of integrated actuators and sensors for attitude determination and control, as well as propulsion system for orbit maneuvers. The GNC algorithms for formation flying, including relative navigation, are computed by the primary host OBC. The body pointing is executed by the integrated ADCS (iADCS) module, which ensures the most precise pointing performance currently possible in a nanosatellite platform.

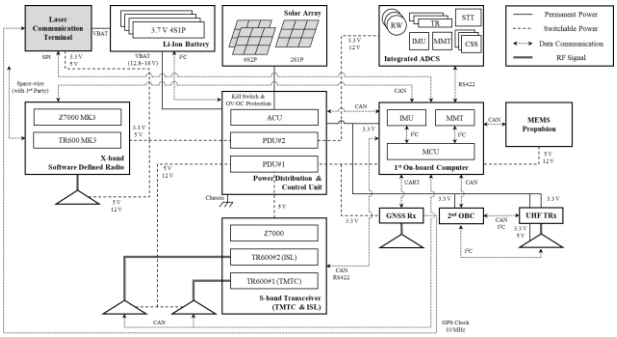

Figure 9: Diagram of the bus electrical interfaces

Figure 10(a) shows the formation flying architecture for the VISION system. Three coarse sun sensor (CSS) arrays are attached to acquire the sun vector. Arcsecond-level attitude determination can be achieved using the star tracker and MEMS gyro. While they carry out the laser crosslink, the LCT provides the AOA to the host OBC and bus corrects LOS errors. The 3-axis RWs are balanced and provide high momentum and torque capacities, having a low jitter characteristic with viscoelastic dampers.[4] The field of uncertainty (FOU) includes the region of the LOS errors yielded by the relative navigation, body pointing, and residual of FSM control. Given the relative navigation and hardware performance, the body pointing is simulated as presented in Figure 10(b). The body pointing errors are smaller than 75 arcsec (3σ) during the PAT sequence, ensuring that the beam spot can stay within the tracking sensors' active area.

The S-band radio system is utilized for sharing GPS signals. For precise estimations, the algorithm corrects the delays induced by data acquisition, parsing, RF crosslinks, etc. Table 2 summarizes the results of the relative navigation for minimum and maximum inter-satellite range. The relative navigation using GPS L1/L2 signals achieves sub-meter accuracy performance by mitigating the ionospheric delays from a long baseline. The propulsion system is utilized for orbit maneuvers which the profiles are generated by the mission planning system on the ground segment. The propulsion system has four MEMS nozzles with a maximum thrust of 1 mN for each nozzle. As presented in Table 3, the total accumulated propellant over the orbit scenario is approximately 5.13 m/s, which is the available propellant budget.

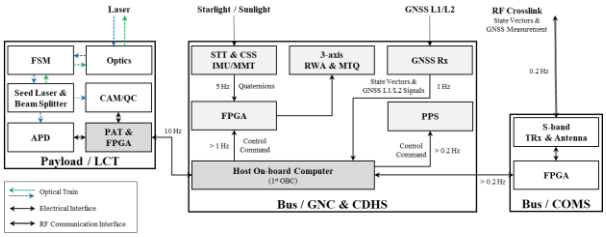

(a) GNC architecture diagram

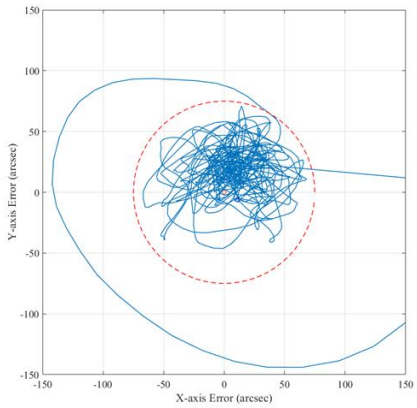

(b) Body-pointing error profile on the X-Y plane

Figure 10: GNC architecture and pointing error

Table 2: Relative navigation simulation results

Range [km]	State	Relative Navigation Error (mean, 3σ)		
50	Pos. [cm] Vel. [cm/s]	0.62±11.50 0.24±0.84	0.03±5.28 −0.00±0.39	0.06±11.59 0.00±0.58
1000	Pos. [cm] Vel. [cm/s]	10.53±24.57 4.79±1.94	0.06±6.30 −0.05±0.53	0.35±89.34 0.02±0.61

Table 3: Summary of the propellant budget

Scenario	Budget [m/s]	ΔV [m/s]	Attempt (times)	Total ΔV [m/s]
Drift Recovery	3.0	2.55	1	2.55
Station Keeping	0.5	0.38	1	0.38
Reconfiguration	2.5	0.11	20	2.20
Residual	0.6	-	-	-
Accumulated ΔV [m/s]	6.6	-	-	5.13

Electrical Power Analysis

The satellites have three solar panels, two deployable and one body-mounted, integrated with highly efficient multiple-junction GaAs cells. They are connected with buck-boost regulators that guarantee a DC-to-DC conversion efficiency of 90%. The orbital average power generation is up to 21.9 W at the EOL. The selected battery pack comprises 4S-2P of lithium-ion cells with 77 Wh capacity and 14.8 V as a nominal voltage. Table 4 summarizes the electrical power budget analysis. For this analysis, the maximum eclipse duration is applied over the mission lifetime. For duty-cycled operations, the average power consumptions are calculated. Given the DC-to-DC conversion efficiency of regulators, the depth of discharge (DOD) for each operation mode is estimated, for which the values are smaller than 20%.

Command and Data Handling Subsystem

The host (or primary) OBC has the following capabilities and features: low-power-consumption embedded RT-patched Linux OS, and GNSS receiver docking. It supports multiple channels for parallel interfaces like CAN-bus and I^2C.

Table 4: Summary of the electrical power budget

Parameter	Operation Scenarios				
	Standby	Maneuver	Mission	Comm.	Safe
Power Gen. [W]	21.64	17.31	17.31	17.31	21.64
Power Draw [W]	5.81	9.29	16.24	9.70	4.47
Discharge [Wh]	−11.71	−16.64	−26.67	−17.37	−9.01
Charge [Wh]	19.76	13.17	13.17	13.17	19.76
Margin [Wh]	8.05	−3.47	−13.50	−4.20	10.75
DOD [%]	-	4.75	18.45	5.74	-

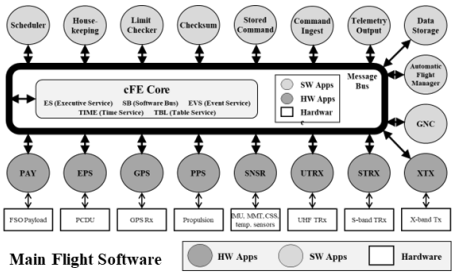

(a) FSW architecture diagram

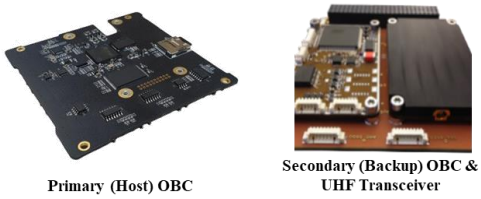

(b) Primary and secondary OBC configurations

Figure 11: FSW architecture and OBC configurations

The cFS is used as the main platform for the FSW. Thus, the FSW has a simplified architecture and is sufficiently robust to provide multi-tasking such as the computation of the formation flying GNC algorithms. With the basic functions in the cFS, the software bus (SB) provides the interface between each module while enhancing of the robustness of the FSW, reducing the development cost. In addition, the backup OBC integrated with the UHF transceiver is adopted to handle on-orbit contingencies, acting as a hardware watchdog timer. The FSW architecture and configurations of two OBCs are displayed in Figure 11.

Communication Subsystem

RF communication transceivers are based on the software-defined radio (SDR), the RF features of which are configurable in orbit. The S-band transceiver includes two modems in a single unit for both TMTC and crosslink, saving internal space and power consumption. UHF communication is adopted for early orbit and backup communication. Finally, X-band communication is available for future applications, but is generally not utilized. To ensure link availability in orbit, the RF link budget analysis was conducted as summarized in Table 5. For both UHF and S-band communications, the link budget should be higher than 6 dB; for X-band, higher than 4 dB. Applying the specifications of each device, the link budget meets the requirements, including the required data rate and modulations. In particular, the S-band crosslink would be available in the range of 1000 km.

Table 5: Summary of the RF link budget

(a) Downlink: UHF, S-band, X-band

Elements	Unit	UHF	S-band (TMTC)	X-band
Modulation	-	GMSK	QPSK	8-PSK
Frequency	MHz	437.0	2200.0	8250.0
Data Rate	kbps	4.8	1000.0	1000000.0
Tx Power	W	1.0	1.0	2.0
Tx Gain	dBi	0.0	8.0	13.0
EIRP	dBm	29.5	37.8	41.7
Path Loss	dB	-153.2	-163.1	-169.5
Rx Gain	dB	18.9	36.0	51.0
Eb/N0	dB	17.3	14.8	14.0
Link Margin	dB	9.6	7.0	4.2

(b) Uplink and crosslink: UHF, S-band

Elements	Unit	UHF	S-band (TMTC)	S-band (Crosslink)
Modulation	-	GMSK	QPSK	QPSK
Frequency	MHz	437.0	2100.0	2200.0
Data Rate	kbps	4.8	500.0	10.0
Tx Power	W	27.0	27.0	1.0
Tx Gain	dBi	18.9	36.0	8.0
EIRP	dBm	57.8	76.3	7.4
Path Loss	dB	-153.2	-162.7	-160.1
Rx Gain	dB	0.0	8.0	8.0
Eb/N0	dB	41.0	37.6	18.6
Link Margin	dB	33.2	29.8	6.7

Structure and Mechanism Subsystem

The structure and mechanism, including the frame and hinge, were designed using aluminum 6061 alloy. The surfaces of these parts will be anodized to prevent cold welding on orbit. Considering the payload integration process, the frame is designed using a skeleton configuration with a high degree of freedom. Given the internal space as depicted in Figure 8(b), the avionics are assembled based on their functions: for example, the stacked boards for CDHS and COMS are located on +Y-axis, and the iADCS is adopted. Conducting the launch environment simulation using the NX10.0 NASTRAN, the first mode frequency with the stowed configuration during the launch phase is analyzed to be above 80 Hz, which is sufficiently higher than the recommended value to avoid resonance with a launch vehicle.

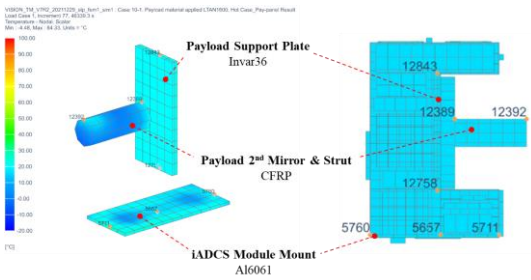

Figure 12: Temperature contour and node ID

Thermal Control Subsystem

For the VISION system, passive thermal control is essentially applied by using an anodized aluminum frame and a black-colored FR-4 PCB. Specially, the battery board includes heaters for heat dissipation, which should maintain the temperature of the battery cells to be above 0 °C. An on-orbit thermal transient simulation for the worst hot and cold cases with seasonal eclipse variations was conducted using NX10.0 Space Thermal Systems. Figure 12 shows the temperature contour and node ID from the thermal analysis. The optical axis misalignment between the payload and iADCS caused by thermal deformation[1] is smaller than 13 μrad, meeting the pointing error budget. The temperature ranges summarized in Table 6 are within the operating temperature, being within the thermal margins with a buffer of at least 10 °C in each case, while the deactivated components are within the survival temperature range.

Table 6: Summary of the thermal analysis results

Subsystem		Operating Temp. (°C)		Worst Case Analysis (°C)	
		Min.	Max.	Min.	Max.
PAY	LCT	−40	+85	20.37	23.71
GNC	iADCS	−20	+50	21.32	22.61
	GNSS Ant	−40	+85	23.41	25.00
	Propulsion	0	+50	20.33	25.40
CDHS	1st OBC (GNSS Rx)	−40	+85	24.28	25.70
	2nd OBC (UHF TRx)	−30	+85	23.81	25.30
COMS	S-band TRx	−40	+85	23.87	25.48
	S-band Ant (TMTC)	−40	+85	11.53	16.09
	S-band Ant (Crosslink)	−40	+85	23.21	24.85
	X-band Tx	−40	+85	20.50	21.48
	X-band Ant	−40	+57	20.38	22.42
	UHF Ant	−40	+85	12.68	17.50
EPS	Solar Panel	−40	+105	−27.83	83.08
	PCDU	−35	+85	21.35	22.40
	Battery	0	+45	20.37	23.74

Preliminary Design Specifications

Table 7 summarizes the preliminary design specifications of the nanosatellites, meeting the requirements for the laser crosslink mission. The mass is 5.66 kg, and dimension satisfies the 6U CubeSat standard. The operation orbit is assumed to be a synchronous orbit of the sun with an LTAN of 18:00 and altitude of 600 km. The GNC system of the bus assists the laser crosslink by precisely correcting the LOS errors. Using GPS L1/L2 signals, the relative navigation system achieves sub-meter accuracy, compensating for the effects due to ionospheric delay from a long baseline. The propellant budget has a margin of approximately 20%, considering a residual at the EOL. The data communications are conducted through CAN-bus interfaces, and the power supply system includes latch-up protection to prevent over-current and over-voltage. RF communication systems consist of S-band, X-band, and UHF radios, meeting the link margin requirements. When they are oriented toward the sun, the power generation is maximized up to 21.9 W at the operation orbit. The power system assures a good battery capability and lifetime from the DOD analysis. The peak current draw is lower than the limitation with any systems operations. The preliminary design ensures that the performance of the nanosatellite bus can support the laser crosslink.

Table 7: Nanosatellite Design Specifications

Parameter	Specifications	Remarks
Operation Orbit	Lifetime > 1 year	-
	Alt. 600 km, LTAN 18:00	Sun-synchronous orbit
Physical Properties	Mass 5.66 kg	< 6 kg (total < 12 kg)
	Size < 0.25×0.12×0.34 m^3	Stowed, 6U standard
GNC	Pointing < 75 arcsec	3σ, LOS error
	Stability < 2 arcsec	1σ, LOS error
	Rel. navigation < 1 m	3σ, each axis
	ΔV (propellant) < 6.6 m/s	10% of residual
Electrical Interface	CAN, SPI, I^2C, RS422, UART	Ethernet, JTAG for debugging
	3.3 V, 5 V, 12 V, VBat (12.8-16 V)	Latch-up protection for each channel
RF Comm.	0.5-2 Mbps/10 kbps	S-band TMTC/crosslink
	90-135 Mbps	X-band mission data
	4.8-9.6 kbps	UHF redundancy
EPS	Generation > 21.9 W	Orbit average
	Draw < 1.7 A	Peak (protected)
	DOD < 18.5%	< 20%
Safety	1st mode freq. > 80 Hz	> 50 Hz (required)
	Margin of safety > 0	Safety factor 1.5

CONCLUSION

This paper provides design schemes for nanosatellites in formation flying for the VISION laser crosslink mission, including mission scenarios and system design specifications. The final goal of the mission is to establish a miniaturized laser crosslink system with Gbps-level super-high-speed inter-satellite data transmission capability at thousands of kilometers. In addition, several space technologies such as deployable optics and precise formation flying can be demonstrated for future applications.

The laser crosslink mission scenarios are summarized from the link access to the maintenance stage. For a feasible optical link design, the practical beam pointing error structure is presented according to the mission scenarios. The nanosatellite systems are designed according to the practical limitations of the COTS-based development. The significance of this study is its contribution to enhancements and advances in spaceborne laser communication systems. The proposed architecture using COTS products will reduce the effort required for system performance evaluation and on-ground verification processes. Moreover, with precise formation flying technologies including orbit maneuver capacities, the proposed systems can be utilized as platforms for LEO mega-constellation applications.

Acknowledgments

This research was supported by the Challengeable Future Defense Technology Research and Development Program (912908601) of the Agency for Defense Development in 2020.

References

1. Long (2018). Pointing Acquisition and Tracking Design and Analysis for CubeSat Laser Communication Crosslinks (Master Thesis). Massachusetts Institute of Technology, USA.
2. Song, Y., Park, S.Y., Kim, G.N., and Kim, D.G., "Design of Orbit Controls for a Multiple CubeSat Mission Using Drift Rate Modulation," Aerospace, vol. 323, No. 8, 2021.
3. Grenfell, P., Serra, P., Cierny, O., Kammere, W., Gunnison, G., Kusters, J., Payne, C., and Cahoy, K., "Design and Prototyping of a Nanosatellite Laser Communications Terminal for the CubeSat Laser Infrared CrosslinK (CLICK) B/C Mission," Proceedings of the 34th Annual Small Satellite Conference, Logan, UT, USA, 2020.
4. Shields, J., Pong, C., Lo, K., Jones, L., Mohan, S., Marom, C., McKinley, I., Wilson, W., and Andrade, L., "Characterization of CubeSat Reaction Wheel Assemblies," Journal of Small Satellites, vol. 6, No. 1, 2017.